

Remaining strength of API J55 steel casing pipes damaged by corrosion

A. Sedmak^a, M. Arsić^b, Ž. Šarkoćević^c, B. Medjo^d, M. Rakin^d, D. Arsić^{e,*}, V. Lazić^e

^a Faculty of Mechanical Engineering, University of Belgrade, Serbia

^b Institute for Testing of Materials (IMS), Belgrade, Serbia

^c Faculty of Technical Sciences, Kosovska Mitrovica, Serbia

^d Faculty of Technology and Metallurgy, University of Belgrade, Serbia

^e Faculty of Engineering, University of Kragujevac, Serbia

ARTICLE INFO

Keywords:

Remaining strength
Casing pipes
Corrosion defect
Maximum allowed pressure
Finite element method

ABSTRACT

Experimental investigation of the integrity of casing pipes, used in the oil drilling rigs, withdrawn after about 70,000 h of service, has been conducted, together with numerical simulation. Pipes were manufactured by the high frequency contact welding (HF) of API J55 steel. The influence of corrosion damage is investigated by means of pressure test of a pipe with different damage levels made by machining the circular holes. The finite element analysis of the damaged pipe subjected to internal pressure is conducted to simulate the stress state in the pipe and to establish the criteria for the maximum pressure that a damaged pipe can withstand. Several analytical expressions were used to estimate the maximum pressure in a damaged pipeline, and the solutions were compared to predictions of finite element models and experimental results.

1. Introduction

Structural integrity is a relatively new scientific and engineering discipline, which also includes analysis of stress-strain state, failure assessment and service life estimate [1–6]. This means that, besides the common situations where integrity needs to be checked after the defect has been discovered, it includes the analysis of the stress state, most often using the finite element method (FEM). In this way it is possible to determine ‘weak’ points in a construction, even before the defect (e.g. crack) has appeared [7–11,43].

The pipelines are the most economical and safest way for oil and gas transport. They can consist of seam or seamless pipes. Pipeline specifications defined by the API 5CT standard mainly include dimensions of the pipes and their joints and mechanical properties. However, reasons that lead to the most frequent failures of the pipelines built from seam pipes are insufficient resistance to crack initiation and propagation and poor quality of the welded joint, as well as reduction of strength caused by the corrosion defects [12–17]. It should be kept in mind that a proper corrosion management in oil and gas industry can help to mitigate a substantial part of corrosion costs [18].

Modern technologies of the welded pipes manufacturing enable a continuous production process with longitudinal and spiral seam, with the main aim of achieving the welding rate equal to the pipe forming

rate. The machines for automatic and semi-automatic manufacturing of the longitudinally welded pipes are mainly constructed for the high frequency welding. The choice of the welding parameters is very important for obtaining the appropriate quality of a welded joint, as shown in Ref. [19,20]. Quality assurance of the welded joints in the manufacturing process of the seam pipes is achieved through the control of all operations during the production of each pipe. By application of the high frequency welding, it is possible to achieve forming rates of up to 50 m/min during the continuous manufacturing of the longitudinally welded pipes.

Casing steel pipes used in the oil drilling rigs are subjected to a corrosive atmosphere making them susceptible to material degradation, often in combination with errors in design and manufacturing. The main concern is the influence of CO₂ and H₂S on the pipelines in the oil and gas exploitation facilities, because these gases at elevated pressures and temperatures (in the presence of water with low pH value) create a very corrosive environment. The steel used for manufacturing the pipes, analysed in this paper, contains approx. 0.1% Cr, which points to its decreased corrosion resistance. Having this in mind, this material is appropriate for oil and gas drilling rigs where CO₂ can be found, while in the case of significant H₂S presence some steel with higher chromium content should be used.

The reliability of the oil and gas drilling rig systems is very important

* Corresponding author. Faculty of Engineering, University of Kragujevac, Sestre Janjić 6 St., 34000, Kragujevac, Serbia.

E-mail address: dusan.arsic@fink.rs (D. Arsić).

<https://doi.org/10.1016/j.ijpvp.2020.104230>

Received 1 July 2020; Received in revised form 3 October 2020; Accepted 6 October 2020

Available online 10 October 2020

0308-0161/© 2020 Elsevier Ltd. All rights reserved.

Table 1
Chemical composition of API J55 steel [mass. %].

C	Si	Mn	P	S	Cr	Ni	Mo	V	Cu	Al	C_{eq}^a
0.29	0.23	0.96	0.013	0.022	0.1	0.058	0.012	0.003	0.13	0.025	0.49

$$^a C_{eq} = [C + Mn/6 + (Cr + Mo + V)/5 + (Ni + Cu)/15] = 0.49.$$

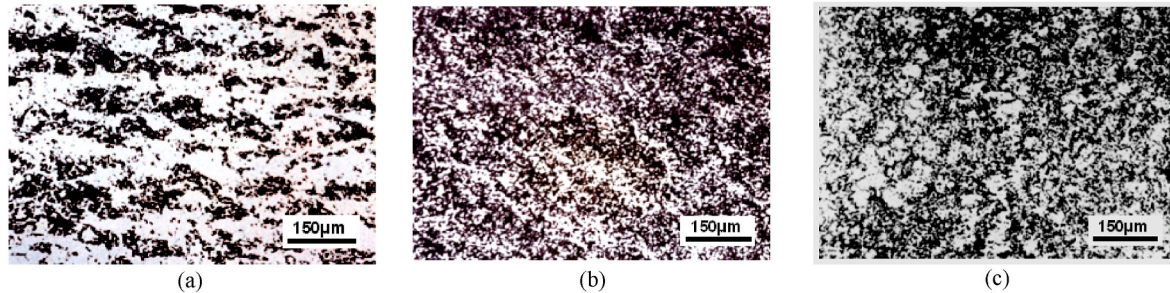


Fig. 1. Microstructure of API J55 steel: a) base metal; b) HAZ, c) weld metal.

Table 2
Tensile properties of API J55 steel, specimens taken from base metal in rolling direction.

Specimen	Temperature	Yield strength	Ultimate tensile strength	Elongation
	[°C]	R_{eH} [MPa]	R_m [MPa]	A [%]
1	20	376	559	33.5
2		384	566	31.4
3		379	562	34.2
Mean value		379.7	562.3	33
Standard API 5CT		379–552	>517	>22.5

for continuous exploitation, but also for the environment protection. Therefore, various methods for estimation of the remaining strength of the pipes with corroded areas exist. Some of the renowned methods deal with the conditions of internal pressure and corrosion at the inner surface, because they are derived by studying the damaged transport pipelines. However, casing pipes can be damaged by corrosion at the inner and/or outer surface and subjected to various loadings, including the external and internal pressure, as well as axial loading (e.g. due to the weight of the construction).

Several procedures and recommendations for assessment of remaining strength of corroded pipelines have been developed [21–32]. One of the procedures for assessment of the corrosion defect influence on the pipe integrity is ASME B31G code [21]. It enables determination of the remaining strength of damaged pipes, by estimating the maximum allowed working pressure. Depending on the corrosion defect length, this code utilizes the parabolic or rectangular defect profile. Having in mind that ASME B31G is often regarded as a too conservative method, several other procedures have been derived, such as modification of B31G by Kiefner and Vieth [22,23], (in the remainder of the text - modified ASME B31G) or RSTRENG. One of the most important changes of the original B31G is approximation of the defect geometry. Some of

the modifications of this procedure, undertaken to increase its accuracy, are given in Ref. [24]. In addition, Det Norske Veritas (DNV) published recommended practice [25], for assessing corroded pipelines integrity under internal pressure and combined internal pressure with longitudinal compressive stress.

In this paper, criteria for evaluation of maximum allowed pressure for damaged casing pipes manufactured from API J55 steel are discussed. The analysed pipe has been in exploitation in an oil drilling rig and was withdrawn after 70,000 h (8 years) of service. Experimental investigation (pressure test) is conducted on a pressure vessel made of a pipe segment, with corrosion defects simulated by machining the circular holes. The vessel was then subjected to the hydrostatic pressure, to determine the spreading of plasticity for analysed damage levels (i.e. depths of the holes). Expressions for calculating the maximum allowed pressure and the finite element method are applied to assess the damaged pipe integrity, and the results are compared and discussed, as well.

2. Material mechanical properties

The results of the chemical composition analysis for API J55 steel, used for fabricating the examined pipe, are given in Table 1. The value of the equivalent carbon content, obtained using the International Institute of Welding (IIW) formula [26], leads to the conclusion that this material is susceptible to cold-cracking.

Microstructure of API J55 steel is shown in Fig. 1, for the base metal, heat-affected-zone (HAZ) and weld metal, revealing different appearances of pearlite-ferrite fine-grain structure.

Tensile properties of API J55 steel were determined using 3 specimens taken from the examined casing pipe. Results are presented in Table 2, together with the API 5CT minimum and maximum values of the yield strength, as well as minimum ultimate tensile strength. Based on testing of new material in different directions, as shown and explained in Ref. [32], one can estimate that the difference in Yield Strength is less than 3%, i.e. negligible. In addition, one should keep in



Fig. 2. Pipe prepared for the pressure testing, a) overall appearance, b) simulated defects on the pipe, with strain gauges mounted.

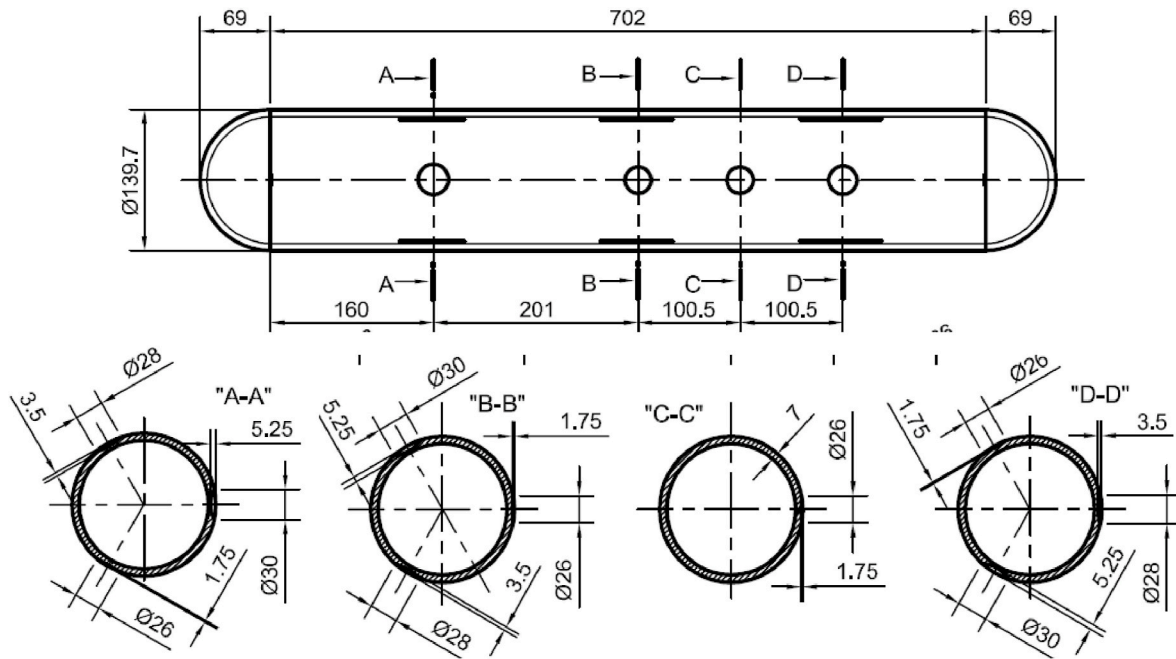


Fig. 3. Positions of the simulated defects on the pipe.

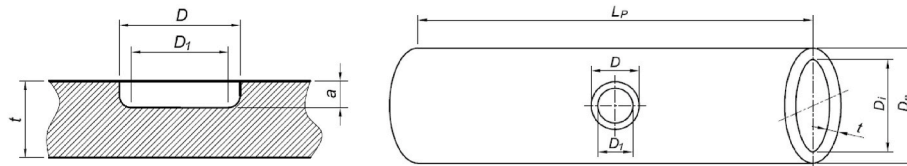


Fig. 4. Dimensions of the simulated defects.

Table 3
Simulated damage levels and dimensions.

Damage level a/t [%]	D [mm]	D_1 [mm]	a [mm]	Point SG & SR
75	30	18	5.25	1, 6–7, 12
50	28	18	3.50	2, 8–9, 10
25	26	18	1.75	3, 4–5, 11 ^a , 13

^a SG11 was not functioning.

mind that results obtained for specimens cut from welded joint are similar to those obtained by testing of the base metal, as a consequence of the fact that HF welds are produced without a filler metal. This was also confirmed by hardness measurement, with the smallest values in the HAZ, but with small differences in the welded joint [32].

3. Experimental procedure

The experimental investigation is conducted on a pressure vessel with defects of the circular shape. The vessel was made from a part of the casing pipe made by the HF welding of API J55 steel, closed at both ends with nominal dimensions: diameter $\varnothing 139.7$ mm, wall thickness 6.98 mm. Although the pipe was subjected to a combination of high pressure and a chemically aggressive environment during the exploitation in the rig, material properties were not seriously deteriorated during this period, as shown in Ref. [32].

The corrosion defects are simulated by machining circular holes at the outer surface of the pipe, Fig. 2b. The depth of these holes is varied, in order to simulate different levels of material loss due to corrosion. Geometry of the analysed pipe and machined holes is shown in Figs. 3

Table 4
Measuring points.

Point	Damage	Cross-section
SG1	$\varnothing 30 \times 5.25$	D-D
SG2	$\varnothing 28 \times 3.5$	D-D
SG3	$\varnothing 26 \times 1.75$	D-D
SR4-5	$\varnothing 26 \times 1.75$	B-B
SR6-7	$\varnothing 30 \times 5.25$	B-B
SR8-9	$\varnothing 28 \times 3.5$	B-B
SG10	$\varnothing 28 \times 3.5$	A-A
SG11	$\varnothing 26 \times 1.75$	A-A
SG12	$\varnothing 30 \times 5.25$	A-A
SG13	$\varnothing 26 \times 1.75$	C-C

and 4, while dimensions of the holes are given in Table 3. Strain gauges (SG) were mounted at the bottom of each hole, to measure the strains in two perpendicular directions, circumferential (hoop) and longitudinal (axial), during the increase of the hydrostatic pressure. Strain gauges LY 11–6/120 and rosettes XY 11–6/120, manufactured by HBM, are used. The measured increase of the strains in these directions during the pressure test, for the three damage levels, is given in Fig. 4. Scheme of measuring points is given in Table 4.

Strain rosetes (SR) 6/120 XY 11 were located at points 4–5, 6–7, 8–9, while other points were equipped with strain gauges 6/120 LY 11. Cross-sections A-A, B-B and D-D had all the three different damage holes, while C-C just one ($\varnothing 26 \times 1.75$) with measuring point 13, Table 4. In line distribution of SG and SR was: line 1: 1-13-(4–5)-10; line 2: 2-(6–7)-11; line 3: 3-(8–9)-12. Results are shown in Table 5, including SG11, which was not functioning.

Table 5
Measured strains (in $\mu\text{m}/\text{m}$) vs. pressure (MPa) - bolded values mark initiation of plastic strain.

Pressure	SG1	SG2	SG3	SR4	SR5	SR6	SR7	SR8	SR9	SG10	SG11 ^a	SG12	SG13
1.0	133	88	68	18	59.9	32.7	133.3	93.89	26	96.29	121.589	146.9	66.19
2.0	280	182	140	35	122.8	65	277.7	193.9	51	198.4	229.834	303.3	130.7
3.0	449	291	223	54	195.3	103	443	308.2	79	315.2	-820.95	481.7	204.5
4.0	592	382	292	70	256.5	134	583	404.9	103	414	-711.54	632.2	266.5
5.0	750	482	369	88	323.5	169	735.9	510.2	129	522	-796.58	797.4	335.4
6.0	904	579	443	106	389.5	203	886.4	613.6	155	627.7	-746.07	959.1	402.3
7.0	1062	679	519	123	456.6	238	1040	718.8	181	735.6	-973.97	1125	471.1
8.0	1226	781	597	142	526.2	273	1198	826.8	208	847.1	-3067.2	1293	540.2
9.0	1392	883	675	161	597.4	310	1356	935.4	235	959.9	1000000	1464	610.7
10.0	1545	977	746	178	663.9	342	1501	1034	259	1065	1000000	1620	674.5
10.5	1620	1023	781	187	697.7	358	1573	1083	271	1117	1000000	1699	706
11.0	1699	1070	817	197	733.3	375	1646	1132	284	1171	1000000	1789	737.8
11.5	1777	1117	852	205	769.1	391	1721	1183	296	1227	1000000	1885	770.6
12.0	1867	1169	892	216	810.2	410	1805	1240	309	1290	1000000	1994	806.8
12.5	1940	1211	923	224	843.8	424	1874	1285	320	1342	1000000	2088	835.4
13.0	2030	1264	962	234	883.1	442	1959	1340	333	1404	1000000	2203	871.1
13.5	2106	1303	990	243	916.2	455	2030	1382	343	1455	1000000	2313	897.7
14.0	2233	1373	1042	256	968.1	480	2149	1456	360	1545	1000000	2479	945.6
14.5	2352	1432	1090	268	1013	499	2258	1518	374	1621	1000000	2638	985.8
15.0	2429	1466	1118	275	1039	511	2325	1555	381	1667	1000000	2766	1009
15.5	2554	1522	1170	286	1080	530	2434	1613	394	1743	1000000	2950	1049
16.0	2695	1578	1232	296	1121	548	2552	1669	406	1844	1000000	3256	1088
16.5	2922	1633	1287	306	1159	566	2665	1724	418	1934	1000000	3455	1128
17.0	3094	1686	1368	316	1197	584	2810	1778	428	2028	1000000	3887	1173
17.5	3312	1747	1424	327	1237	608	2951	1839	443	2125	1000000	4168	1217
18.0	3716	1820	1507	340	1285	632	3150	1935	463	2296	1000000	4620	1269
18.5	4468	1994	1624	358	1354	671	3481	2070	489	2590	1000000	5555	1349
19.0	5450	2223	1759	381	1436	715	3962	2298	529	2885	1000000	6718	1443
19.5	6010	2356	1852	393	1480	739	4254	2424	553	3110	1000000	7416	1494
20.0	6510	2465	1930	403	1519	765	4540	2570	578	3268	1000000	8023	1540
20.5	7184	2608	2010	417	1570	794	4932	2774	605	3503	1000000	8908	1602
21.0	7719	2737	2066	427	1604	816	5224	2927	620	3662	1000000	9561	1643
21.5	8334	2909	2153	438	1646	841	5590	3136	642	3902	1000000	10328	1689
22.0	8963	3024	2234	450	1688	875	6048	3450	662	4140	1000000	11055	1737
22.5	10161	3354	2417	473	1774	920	6915	3971	680	4677	1000000	12606	1844
23.0	11466	3711	2585	504	1893	979	8044	4688	701	5309	1000000	14159	1980
23.5	12511	3971	2764	522	1983	1040	8922	5245	713	5816	1000000	15343	2071
24.0	13205	4171	2886	534	2055	1089	9472	5592	719	6153	1000000	16064	2121
24.5	13464	4258	2937	541	2091	1107	9696	5758	716	6301	1000000	16352	2135
25.0	14353	4600	3117	554	2275	1191	10594	6332	727	6856	1000000	17476	2284
25.5	15898	5190	3407	581	2517	1333	12123	7320	749	7784	1000000	19331	2512
26.0	17776	5862	3823	615	2746	1526	13842	8475	755	8837	1000000	21445	2905
26.5	20068	6695	4325	645	3088	1782	15820	9816	759	10070	1000000	/	3314
27.0	/	7670	4962	670	3505	2174	18313	11452	771	11573	-23551	/	3791
27.5	/	8202	5332	691	3714	2412	19659	12314	783	12468	-23256	/	4060
28.0	/	8792	5788	722	3979	2696	21232	13367	812	13519	-22874	/	4341
28.5	/	9604	6409	755	4290	3105	/	14934	937	14834	-22446	/	4726
29.0	/	10758	7362	791	4892	3701	/	17170	/	16740	-21645	/	5386
29.5	/	12417	8633	822	5912	4505	/	19483	/	19081	-20562	/	6774
30.0	/	13916	9562	861	6827	5114	/	1E+06	/	20772	-19716	/	8539
30.5	/	14744	10157	784	8108	5941	/	1E+06	/	22029	-19397	/	11101
31.0	/	10806	7434	268	5840	4572	/	19137	/	17652	-21225	/	8691

^a SG11 was not functioning.

The comparison of the hoop strains (mean values from the two strain gauges for each damage level, Table 5) is given for $p = 26$ MPa, damage level 75% (SG1 and SG2, 0.195%), damage level 50% (SG2 and SG10, 0.074%), damage level 25% (SG3 and SG13, 0.034%). It can be seen that the strain at the bottom of 75% defect is cca 2.6 times larger in comparison to the defect of 50% and cca 5.8 times larger in comparison to the defect of 25%. One can notice good agreement between strains in circumferential and longitudinal direction, up to the yield point, i.e. $1610 \mu\text{m}/\text{m} = 0.0161 = 380/210000 (R_{eH}/E)$, following the ratio $\varepsilon_y/\varepsilon_x = 4.25$, as theoretically predicted for bi-axial stress state [23]: $E\varepsilon_x = 0.2 pR/t$, $E\varepsilon_t = 0.2 pR/t$, where ε_x is longitudinal strain, ε_t circumferential strain. Also, to be noticed is the fact that readings from SG 12 and SG10 are somewhat larger than for SG1 and SG2 in elasticity, and up to 25% in plasticity.

$$\begin{aligned} \text{longitudinal : } E\varepsilon_x &= 0, 2 \cdot \frac{pR}{t}, \\ \text{circumferential : } E\varepsilon_t &= 0, 85 \cdot \frac{pR}{t}. \end{aligned}$$

Measured strains are also shown in Figs. 5–7, indicating elastic-plastic behaviour around all the three damage regions, as well as comparison of the mean strain values in Fig. 8. Differences in strain gauges' readings (Figs. 5–7) can be attributed to the different local positions with respect to the damage site.

Plastic strain distribution, as indicated in Table 5 and shown in Figs. 5–8, needs some further clarification, especially in respect to pressure when they initiate (cca 10.5 MPa for 25% damage, 15.5 MPa for 59% and 19.5 MPa for 75%). If these values are compared with values according to yield strength (380 MPa), radius (69.85 mm) and remaining thickness (5.25 mm for 25% damage, 3.5 mm for 50%, and 1.75 mm for 75%), being 28.5 MPa, 19 MPa and 9.5 MPa, respectively, one can see that damage effect is less pronounced for larger damage, since FEM predicts higher pressure for 75% damage (10.5 MPa vs. 9.5 MPa), and lower pressure for 25% and 50% damage (19.5 MPa vs. 28.5 and 15.5 MPa vs. 19 MPa, respectively). One can also notice that the effect of 50% damage is closer to the smaller damage than to the

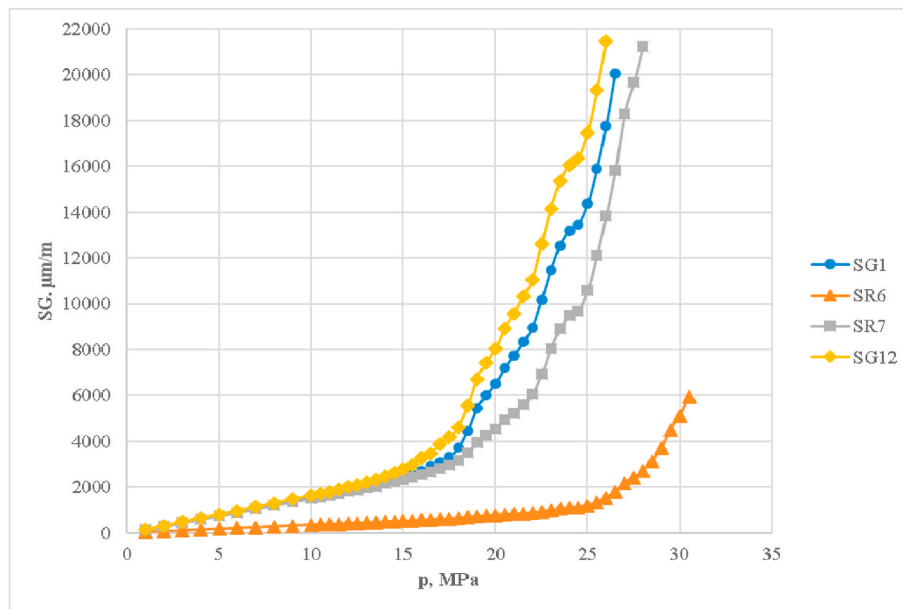


Fig. 5. Measurement of strain gauges positioned at 75% damage.

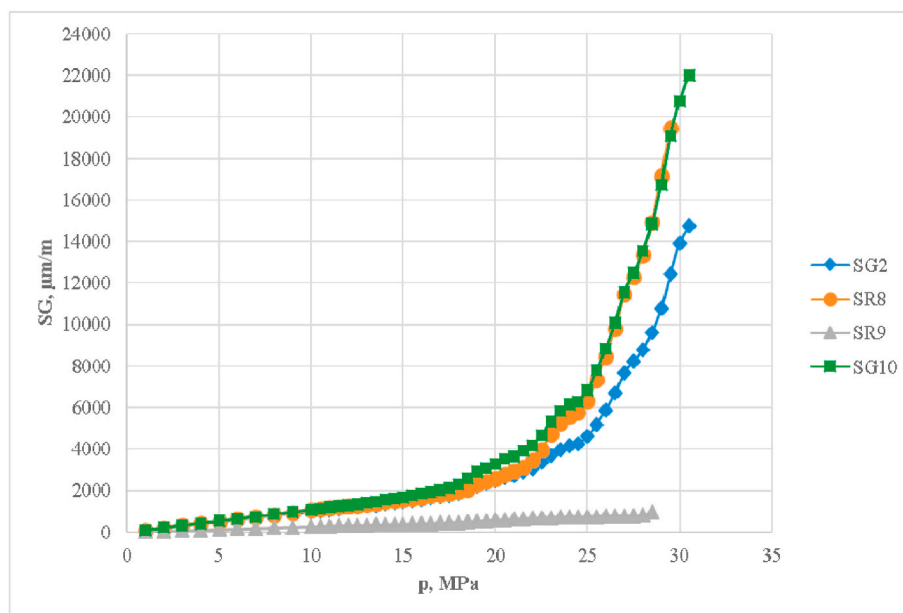


Fig. 6. Measurement of strain gauges positioned at 50% damage.

larger one.

4. Finite element model

Numerical analysis of behaviour of the pipe with machined defects under external loading (hydrostatic pressure) is conducted using the three-dimensional (3D) elastic-plastic finite element method (FEM), as described in Ref. [33–41]. The meshes with defects 25, 50 and 75% of the pipe wall thickness consist of 20-node reduced integration elements, and are shown in Fig. 9. Software package ABAQUS is used for the model creation, processing and postprocessing of the results. Due to the symmetry, one quarter of the pipe is modelled, with appropriate symmetry boundary conditions defined at the model boundaries. The loading is defined by prescribing the hydrostatic pressure at the inner side of the pipe, in accordance with the experimental procedure. To take into

account the fact that the pipe was capped at both ends for experimental investigation, appropriate axial loading is introduced at one end of the FE model. Having in mind that the strains are measured in the center of each defect, in numerical analysis these values are determined in the finite element nearest to that location. This element is marked in Fig. 9, for 25% defect and the results are determined in the integration point nearest to the middle of the defect.

The pipe was modelled using the properties of the base material only. Such a simplification is supported by the fact that the properties of the base material and welded joint, determined on the samples taken from a new (as-received) pipe, did not exhibit significant differences (less than 3%), as show in Ref. [24].

The distribution of von Mises equivalent stress in the vicinity of the 50% defect is shown in Fig. 10 and in more detailed view in Fig. 11, indicating the value just above the yield stress (386.8 MPa compared to

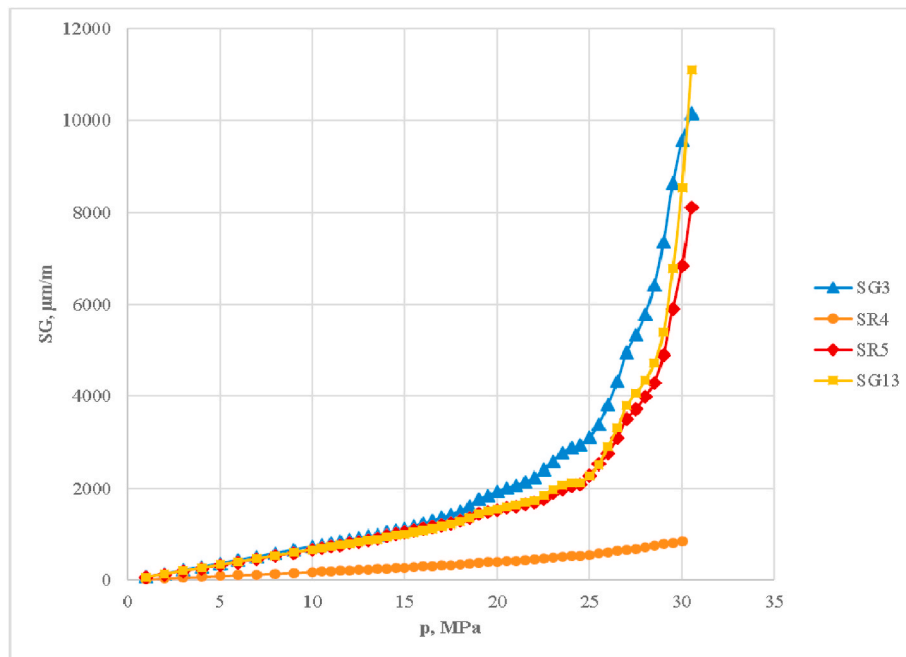


Fig. 7. Measurement of strain gauges positioned at 25% damage.

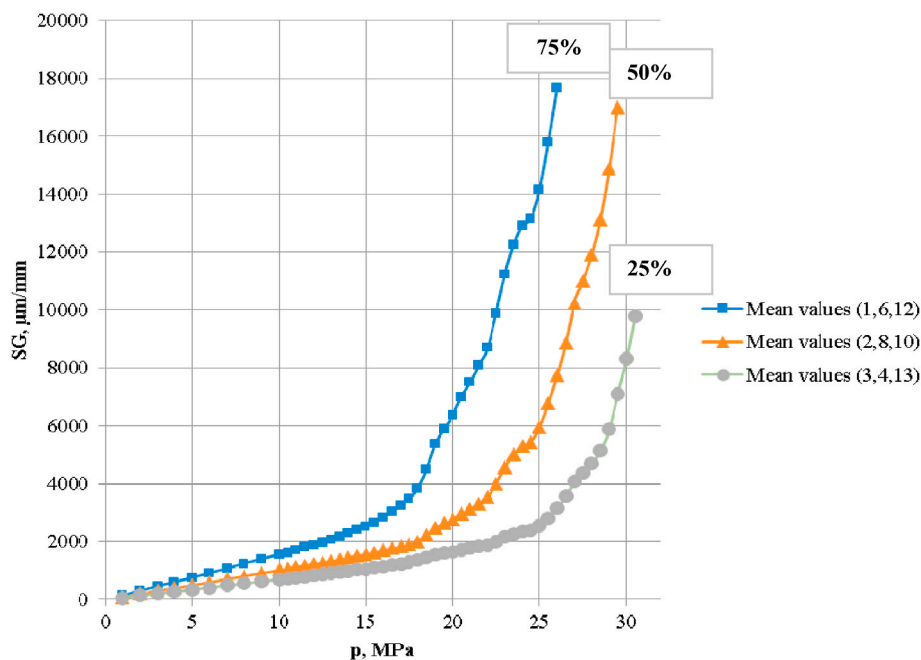


Fig. 8. Mean values of measurements at 75%, 50% and 25% damage.

380 MPa). Comparing this value with the maximum strain for the same point (SG10, cca 2.07%, corresponding to the yield plateau, Fig. 2), one can see very good agreement between experimental and numerical results.

5. Maximum allowed pressure of the corroded pipe

Several well-known solutions from the literature are applied for calculation of the maximum allowed pressure of the analysed API J55 steel casing pipe; in addition to ASME B31G code, modified ASME B31G and the solution of Choi et al. [30] are used. These three expressions are

shown in Table 6. The pipe dimensions and a simulated defect are shown in Fig. 3.

In Table 6, a and L are defect depth and length, M respectively, is geometry correction factor, while C_j ($j = 0.2$) are coefficients in Choi's equation. Geometry of the pipe is defined in Fig. 3; D_e and D_i represent the external and internal diameter of the pipe respectively, $D_i = D_e - 2t$, while mean pipe radius is $R = (D_e + D_i) / 4$. The length of the defect L , used in the original expressions, is replaced by the diameter of defect, D . Although with different shape compared to defects analysed in Table 6, this is still reasonable and conservative approximation, since the shape of actual defects is rounded, producing lower stress concentration than

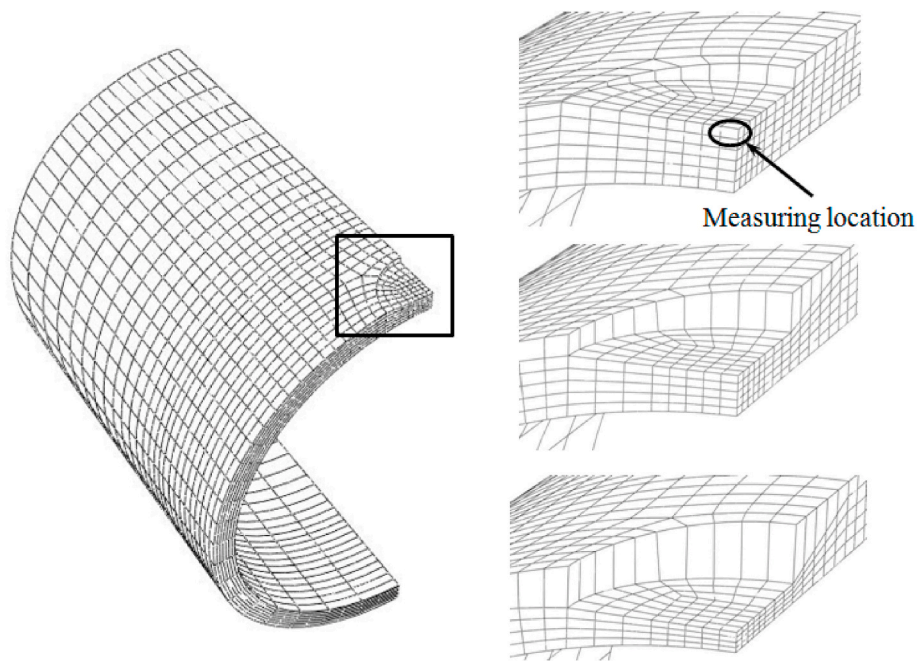


Fig. 9. Finite element mesh with magnified details around the defects with depth 25%, 50% and 75%.

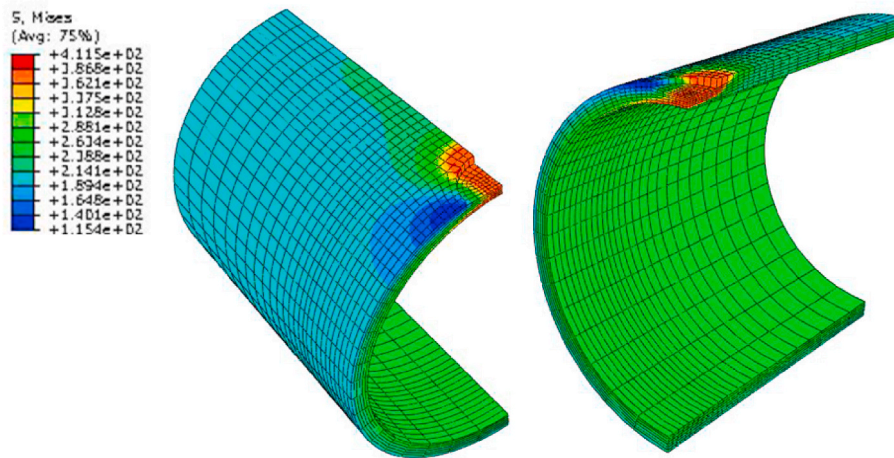


Fig. 10. Distribution of von Mises equivalent stress for the 50% defect, pressure 30 MPa.

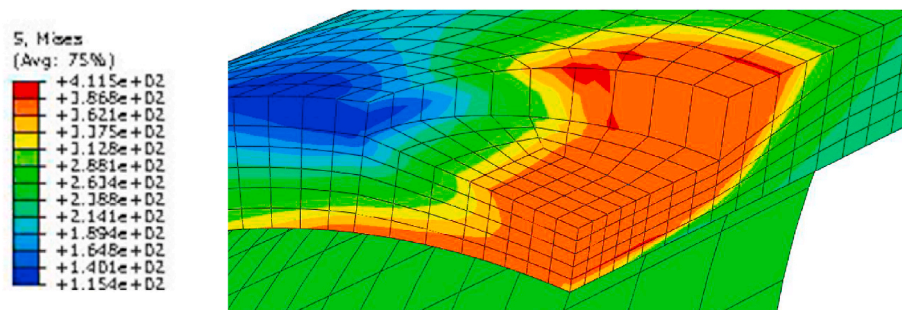


Fig. 11. Distribution of von Mises equivalent stress for the 50% defect – detail.

the shape assumed in Choi's equation.

As a preliminary check of acceptability of the analysed defects, the criterion from ASME B31G code, shown in Fig. 12, is applied. According to this criterion, damaged pipes should withstand the pressure which

produces the hoop stress equal to the yield strength (parabolic line in Fig. 12). The ordinate of this diagram represents the maximum defect depth a divided by the pipe wall thickness t , while the abscissa values are obtained as the ratio of defect length in the longitudinal direction L

Table 6
Expressions used for calculation of the maximum allowed pressure.

ASME B31G		
$L \leq \sqrt{20 \cdot D_e t}$	$p_{max} = 1.1 \cdot \sigma_Y \frac{2t}{D_e} \left[\frac{1 - \frac{2a}{3t}}{1 - \frac{2a}{3t} \frac{1}{M}} \right]$	$M = \sqrt{1 + 0.8 \frac{L^2}{D_e t}}$
$L > \sqrt{20 \cdot D_e t}$	$p_{max} = 1.1 \cdot \sigma_Y T \frac{2t}{D_e} \left(1 - \frac{a}{t} \right)$	$M = \infty$
Modified ASME B31G		
$L \leq \sqrt{50 \cdot D_e t}$	$p_{max} = (1.1 \cdot \sigma_Y + 69 \cdot 10^6) \frac{2t}{D_e} \left(\frac{1 - 0.85 \frac{a}{t}}{1 - 0.85 \frac{a}{t} \frac{1}{M}} \right)$	$M = \sqrt{1 + 0.6275 \frac{L^2}{D_e t} - 0.003375 \left(\frac{L^2}{D_e t} \right)^2}$
$L > \sqrt{50 \cdot D_e t}$		$M = 3.3 + 0.032 \frac{L^2}{D_e t}$
Choi's solution		
$L < 6\sqrt{Rt}$	$p_{max} = 0.9 \cdot \sigma_m \frac{2t}{D_i} \left[C_2 \left(\frac{L}{\sqrt{Rt}} \right)^2 + C_1 \left(\frac{L}{\sqrt{Rt}} \right) + C_0 \right]$	$C_2 = 0.1163 \left(\frac{a}{t} \right)^2 - 0.1053 \left(\frac{a}{t} \right) + 0.0292$ $C_1 = -0.6913 \left(\frac{a}{t} \right)^2 + 0.4548 \left(\frac{a}{t} \right) - 0.1447$ $C_0 = 0.06 \left(\frac{a}{t} \right)^2 - 0.1035 \left(\frac{a}{t} \right) + 1.0$
$L \geq 6\sqrt{Rt}$	$p_{max} = \sigma_m \frac{2t}{D_i} \left[C_1 \left(\frac{L}{\sqrt{Rt}} \right) + C_0 \right]$	$C_1 = 0.0071 \left(\frac{a}{t} \right) - 0.0126$ $C_0 = -0.9847 \left(\frac{a}{t} \right) + 1.1101$

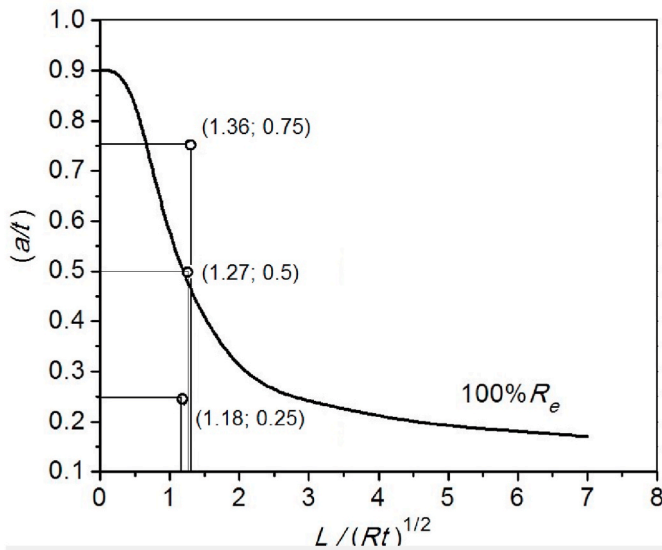


Fig. 12. Criterion for defect acceptance, according to ASME B31G.

(here, L is equal to diameter of the defect, i.e. 30, 28 and 26 mm) and square root of the mean pipe radius R multiplied by t . Having in mind that these values represent only geometry (of the pipe and the defect), each defect can be represented by a single point on the diagram. Acceptable defect dimensions are located below and on the left side of the continuous line for the hoop stress. It is obvious that the defect with depth 25% do not affect the pipe integrity, 75% defect fall within the critical state of the pipe, while 50% defect can be regarded as the limit of acceptability according to ASME B31G criterion, which is considered to be rather conservative [32].

6. Failure criterion

Results obtained using the FEM with different reference stress (80%, 85% and 90% of the ultimate tensile strength) and expressions from Table 6 for maximum allowed pressure in a damaged pipeline are shown in Table 7 for different damage levels. When considering the finite element solutions, failure criterion is considered to be fulfilled when von Mises stress value reaches the reference stress through the entire ligament.

Table 7
Maximum allowed pressure – analytical solutions and FEM with different reference stress.

Damage level	Maximum allowed pressure [MPa]					
	ASME B31G	Modified ASME B31G	Choi's solution	FEM 0.85	FEM 0.8	FEM 0.9
25%	39.8	46.1	50.2	50.5	48.6	51.8
50%	37.1	42.1	48.2	44.8	43.7	45.6
75%	32.9	34.8	39.6	36.9	35.8	37.9

Having in mind that the length of the defect (in addition to its depth) also affects the maximum allowed pressure for the pipe, cases with increased defect length have been also investigated [27]. The predictions of this pressure value for the three used methods are given in Fig. 13, for different defect lengths (i.e. ratio L/\sqrt{Rt}). A model of such a defect (with depth 75% of the pipe wall thickness and L/\sqrt{Rt} value equal to 5), together with all the details of this analysis, is presented in Ref. [25]. Prediction, obtained using the FEM and the same failure criterion as before, is closer to the result of Choi's equation, Fig. 13a, i.e. this equation gives more conservative results for long and deep defects. Its conservatism, in comparison to modified ASME B31G, for long damages is also shown in Ref. [30], for API X65 steel pipes.

On the other hand, when considering long defects with small depth, it can be seen (Fig. 13b) that Choi's equation gives an increase of the predicted failure pressure with the increase of defect length. In that case, use of modified ASME B31G gives a more conservative solution. However, the increase in maximum pressure does not exist for slightly deeper defects (more than 35% of the pipe wall thickness).

7. Conclusions

Based on the obtained results, the following conclusions are drawn:

- According to the ASME B31G criterion for defect acceptance, the integrity of the analysed pipe with defect at the outer surface is not endangered if depth of the defect is less than 50% of the pipe wall thickness. This indicates, together with other, more sophisticated results, high capability of pipes to sustain relatively large defects, also pointing out the possibility of repair crack-like defects in a manner described in Ref. [42].

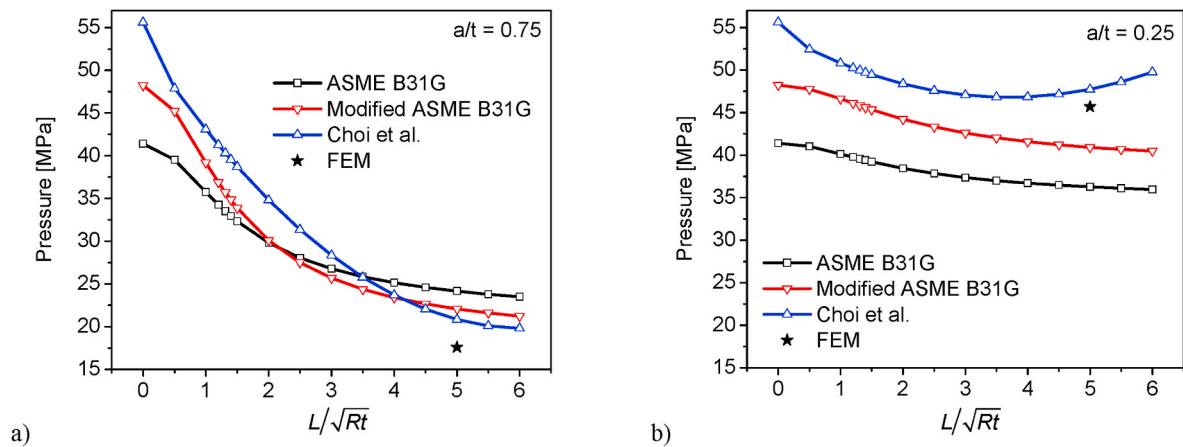


Fig. 13. Comparison of the maximum allowed pressures for defects with depth: a) 75%, b) 25% of the pipe thickness.

- Compared with ASME B31G criterion, including modified one, Choi's equation is less conservative, except for long and deep defects. In that case, modified ASME B31G is also more conservative than original ASME B31G criterion, but less than Choi's.
- The FEM results for stresses and strains are verified by experimental ones, since the agreement between them is excellent, even better than the agreement between readings of different strain gauges themselves. Anyhow, as for the FEM prediction of failure, one should keep in mind that it strongly depends on the reference stress.
- The FEM provides values in-between ASME B31G and Choi's criterion, except for a long and deep defect, where significantly more conservative values are obtained. This might also indicate that the limits of validity for analytical solutions are overestimated.

CRediT authorship contribution statement

A. Sedmak: Conceptualization, Writing - original draft. **M. Arsić:** Conceptualization, Methodology, Resources. **Ž. Šarkočević:** Investigation. **B. Medjo:** Software. **M. Rakin:** Software, Validation. **D. Arsić:** Writing - review & editing. **V. Lazić:** Supervision.

Declaration of competing interest

The authors declare that they have no known competing financial interests or personal relationships that could have appeared to influence the work reported in this paper.

Acknowledgements

Financial support from the Serbian Ministry of Education, Science and Technological development is acknowledged.

References

- [1] M. Katinić, D. Kozak, I. Gelo, D. Damjanović, Corrosion fatigue failure of steam turbine moving blades: a case study, *Eng. Fail. Anal.* 106 (2019), <https://doi.org/10.1016/j.engfailanal.2019.08.002>. Article Number: 104136.
- [2] V. Pilić, V. Mihajlović, P. Stanojević, A. Anđelković, D. Baloš, Application of innovative risk assessment methodology for damage mechanisms identification on part of amine regeneration unit, *Structural Integrity and Life* 19 (1) (2019) 29–35.
- [3] R. Zaidi, A. Sedmak, S. Kirin, A. Grbović, W. Li, LjL. Vulićević, Z. Šarkočević, Risk assessment of oil drilling rig welded pipe based on structural integrity and life estimation, *Eng. Fail. Anal.* 112 (2020), <https://doi.org/10.1016/j.engfailanal.2020.104508>. Article No: 104508.
- [4] M. Mokhtari, R.E. Melchers, Next-generation fracture prediction models for pipes with localized corrosion defects, *Eng. Fail. Anal.* 105 (2019) 610–626.
- [5] M. Katinić, D. Kozak, Z. Božić, I. Gelo, Plastic limit pressures for cracked tube containing twin collinear axial through-wall cracks, *Arch. Appl. Mech.* 89 (5) (2019) 805–811.
- [6] R. Nikolić, D. Arsić, A. Arsić, Ž. Šarkočević, D. Cvetković, B. Hadzima, The fault tree analysis of causes of the welded pipes failures in exploitation, *Communications - Sci. Letters Univ. Žilina* 22 (1) (2020) 62–70.
- [7] A. Sedmak, M. Rakin, Application of fracture mechanics in assessment of structural integrity, in: S. Sedmak, Z. Radaković (Eds.), *Monograph of the 8th International Fracture Mechanics Summer School - from Fracture Mechanics to Structural Integrity Assessment*, DIVK-TMF, Belgrade, 2004, pp. 373–386. Accessible from, www.structuralintegrity.eu.
- [8] A. Okodi, M. Lin, N. Yoosef-Ghods, M. Kainat, S. Hassani, S. Adee, Crack propagation and burst pressure of longitudinally cracked pipelines using extended finite element method, *Int. J. Pres. Ves. Pip.* 184 (2020) 104115, <https://doi.org/10.1016/j.ijpvp.2020.104115>.
- [9] D. Kozak, Z. Ivandić, P. Konjatić, Determination of the critical pressure for a hot-water pipe with a corrosion defect, *Materiali in Tehnologije* 44 (6) (2010) 385–390.
- [10] M. Saravanan, S. Vishnuvardhan, P. Gandhi, G. Raghava, A. Khan, V. Bhasin, J. Chattopadhyay, Fracture studies on carbon steel straight pipes having off-centred circumferential through-wall crack under finite compliance, *Int. J. Pres. Ves. Pip.* 182 (2020), <https://doi.org/10.1016/j.ijpvp.2020.104077>. Article No: 104077.
- [11] B. Medjo, M. Arsić, M. Mladenović, Z. Savić, V. Grabulov, Z. Radosavljević, M. Rakin, Influence of defects on limit loads and integrity of the pipeline at hydropower plant 'PIROT', *Structural Integrity and Life* 20 (1) (2020) 82–86.
- [12] S. Kirin, A. Sedmak, R. Zaidi, A. Grbović, Ž. Šarkočević, Comparison of experimental, numerical and analytical risk assessment of oil drilling rig welded pipe based on fracture mechanics parameters, *Eng. Fail. Anal.* 114 (2020), <https://doi.org/10.1016/j.engfailanal.2020.104600>. Article No: 104600.
- [13] M. Askari, M. Aliofkhaezrai, S. Afroukhteh, A comprehensive review on internal corrosion and cracking of oil and gas pipelines, *J. Nat. Gas Sci. Eng.* 71 (2019), <https://doi.org/10.1016/j.jngse.2019.102971>. Article No: 102971.
- [14] A.H. Alamri, Localized corrosion and mitigation approach of steel materials used in oil and gas pipelines – an overview, *Eng. Fail. Anal.* 116 (2020), <https://doi.org/10.1016/j.engfailanal.2020.104735>. Article number: 104735.
- [15] H.R. Vanaei, A. Eslami, A. Egbewande, A review on pipeline corrosion, in-line inspection (ILI), and corrosion growth rate models, *Int. J. Pres. Ves. Pip.* 149 (2017) 43–54.
- [16] U. Bhardwaj, A.P. Teixeira, C. Guedes Soares, Uncertainty in reliability of thick high strength pipelines with corrosion defects subjected to internal pressure, *Int. J. Pres. Ves. Pip.* 188 (2020), <https://doi.org/10.1016/j.ijpvp.2020.104170>. Article No: 104170.
- [17] B. Chegeni, S. Jayasuriya, S. Das, Effect of corrosion on thin-walled pipes under combined internal pressure and bending, *Thin-Walled Struct.* 143 (2019), <https://doi.org/10.1016/j.tws.2019.106218>. Article No: 106218.
- [18] M. Eskandarzade, A. Kalaki, R. Shahriver, The application and limitations of corrosion management process, *Struct. Integr. Life* 18 (3) (2018) 159–162.
- [19] V. Lazić, D. Arsić, R. Nikolić, D. Rakić, S. Aleksandrović, M. Dordević, B. Hadzima, Selection and analysis of material for boiler pipes in a steam plant, *Procedia Eng.* 149 (2016) 216–223.
- [20] Ž. Šarkočević, M. Arsić, M. Rakin, A. Sedmak, Fabrication of welded tubes by high strength steel and quality indicators, *Structural Integrity and Life* 8 (2008) 81–98.
- [21] American Society of Mechanical Engineers, ASME B31G: Manual for Determining the Remaining Strength of Corroded Pipelines, The Society, New York, 1991.
- [22] J. Kiefner, P. Vieth, A modified criterion for evaluating the strength of corroded pipe. Final Report on Project PR 3-805 to the Pipeline Supervisory Committee of the American Gas Association, Battelle, Ohio, 1989.
- [23] J. Kiefner, P. Vieth, Evaluating pipe-1 new method corrects criterion for evaluating corroded pipe, *Oil Gas J.* 88 (1990) 56–59.
- [24] D.S. Cronin, R.J. Pick, A new multi-level assessment procedure for corroded line pipe, in: *Proceedings of the International Pipeline Conference*, 2000, pp. 801–808. Calgary.

- [25] Det Norske Veritas DNV Rp-F101, Corroded Pipelines - Recommended Practice, The Society, Hovik, 2004.
- [26] V. Lazić, D. Arsić, Nikolić Ružica, D. Djordjević, R. Prokić-Cvetković, O. Popović, Application of the high strength steel HARDOX 450 for manufacturing of Assemblies in the Military industry, *Key Eng. Mater.* 755 (2017) 96–105.
- [27] P. Hopkins, D.G. Jones, A study of the behavior of long and complex-shaped corrosion in transmission pipelines. British Gas Plc, 1992. OMAE-92-1004.
- [28] K. Kueter, OPC Tubing Corrosion, Internal Memorandum of Occidental Oil and Gas, 1992.
- [29] D.R. Stephens, B.N. Leis, J.D. Kurre, D.L. Rudland, Development of an alternative failure criterion for residual strength of corrosion defects in moderate- to high-toughness pipe. Battelle report to PRC International Report, 1999. AGA Catalog Number L51794.
- [30] J.B. Choi, B.K. Goo, J.C. Kim, Y.J. Kim, W.S. Kim, Development of limit load solutions for corroded gas pipelines, *Int. J. Pres. Ves. Pip.* 80 (2003) 121–128.
- [31] O. Enyinnaya, E. Ubong, S. Jerzy, Relationship between microstructural features in pipeline steel and hydrogen assisted degradation, *Eng. Fail. Anal.* 96 (2019) 496–507.
- [32] Z. Šarkočević, M. Arsić, B. Medjo, D. Kozak, M. Rakin, Z. Burzić, A. Sedmak, Damage level estimate of API J55 steel for welded seam casing pipes, *Strojarsstvo: J. Theor. Appl. Mech. Eng.* 51 (2009) 303–311.
- [33] Z. Radaković, M. Abukhres, A. Sedmak, I. Ivanović, B. Petrovski, Direct measurement of the J integral on a pressure vessel, *Struct. Integr. Life* 13 (3) (2013) 163–169.
- [34] A. Sedmak, Computational fracture mechanics: an overview from early efforts to recent achievements, *Fatig. Fract. Eng. Mater. Struct.* 41 (2018) 2438–2474, <https://doi.org/10.1111/ffe.12912>.
- [35] B. Medjo, M. Rakin, M. Arsić, Ž. Šarkočević, M. Zrilić, S. Putić, Determination of the load carrying capacity of damaged pipes using local approach to fracture, *Mater. Trans.* 53 (1) (2012) 185–190.
- [36] I. Dimić, M. Arsić, B. Medjo, A. Stefanović, V. Grabulov, M. Rakin, Effect of welded joint imperfection on the integrity of pipe elbows subjected to internal pressure, *Teh. Vjesn.-Tech. Gaz.* 20 (2) (2013) 285–290.
- [37] LjL. Vuličević, M. Arsić, Ž. Šarkočević, A. Sedmak, M. Rakin, Structural life assessment of oil rig pipes made of API J55 steel by high frequency welding, *Teh. Vjesn.-Tech. Gaz.* 20 (6) (2013) 1091–1094.
- [38] B. Medjo, M. Rakin, N. Gubeljak, Y. Matvienko, M. Arsić, Z. Šarkočević, A. Sedmak, Failure resistance of drilling rig casing pipes with an axial crack, *Eng. Fail. Anal.* 58 (2015) 429–440.
- [39] M. Rakin, B. Medjo, M. Arsić, Z. Šarkočević, A. Sedmak, Effect of exploitation conditions and flaw geometry on the load carrying capacity of casing pipes for oil drilling rigs, *Key Eng. Mater.* 488–489 (2012) 577–580.
- [40] M. Rakin, B. Medjo, M. Arsić, Z. Šarkočević, I. Ivanović, A. Sedmak, API J55 steel casing pipe with an initial surface crack under internal pressure - determination of fracture parameters, *Key Eng. Mater.* 488–499 (2012) 577–580.
- [41] M. Rakin, M. Arsić, B. Medjo, Z. Šarkočević, A. Sedmak, Structural integrity assurance of casing pipes in the oil and gas industry, *WIT Trans. Built Environ.* 134 (2013) 401–410.
- [42] A. Milovanović, A. Sedmak, N. Gnjatović, Application of Fracture Mechanics Parameters to Spherical Storage Tank Integrity Assessment, *Teh. Vjesn.-Tech. Gaz.* 27 (5) (2020) 1592–1596.
- [43] M. Sadou, M. Hadj Meliani, M. Amara, BGN. Muthanna, N. Merah, RK. Suleiman, Impact resistance of API 5L steel in aggressive environment with the presence of green inhibitors, *Struct. Integr. Life* 20 (1) (2020) 57–62.